Binding of L-Arginine and Imidazole Suggests Heterogeneity of Rat Brain Neuronal Nitric Oxide Synthase†

Antonius C. F. Gorren,* Kurt Schmidt, and Bernd Mayer

Institut für Pharmakologie und Toxikologie, Karl-Franzens-Universität Graz, Universitätsplatz 2, A-8010 Graz, Austria

Received February 13, 2002; Revised Manuscript Received April 12, 2002

ABSTRACT: Nitric oxide synthase (NOS) is inhibited by imidazole, which binds to the heme in a low-spin complex absorbing at 428 nm. Conversion by L-arginine of this complex into a high-spin species absorbing at 395 nm is a common method to determine the binding parameters of Arg. However, both Arg-competitive and noncompetitive inhibition of NOS by imidazole has been reported, and optical studies with neuronal NOS provided no evidence for imidazole affecting Arg binding. We investigated the cause for these paradoxical observations with recombinant rat brain neuronal NOS. Imidazole bound to nNOS with a K_d^{app} of 50 μM; tetrahydrobiopterin (BH4) lowered the affinity of nNOS for imidazole 4-fold. The enzyme behaved heterogeneously with respect to Arg binding. Most of nNOS (65−80%) showed competition between Arg and imidazole. In the presence of BH4, a K_d(Arg) of 1 μM could be estimated for this fraction, as well as apparent association and dissociation rate constants of 2.5×10^6 $M^{-1}\cdot s^{-1}$ and 2.5 s^{-1}. A second fraction of nNOS (20−30%) exhibited little or no competition. Consequently, Arg binding did not cause dissociation of the imidazole complex for this fraction, and complete generation of the high-spin state by Arg could not be achieved in the presence of imidazole. A third fraction (≤10%) bound Arg with low affinity (K_d 1−2 mM). Because of this heterogeneity, titration curves with Arg became almost uninterpretable. We propose that this heterogeneous response of nNOS toward Arg and imidazole is underlying the apparently conflicting results reported in the literature.

Nitric oxide synthase (EC 1.14.13.39; NOS)[1] generates NO and L-citrulline from L-arginine, O_2, and NADPH-derived electrons (for reviews see refs *1*−*6*). There are three well-established isoforms of the enzyme: neuronal, endothelial, and inducible NOS (nNOS, eNOS, and iNOS). All isoforms consist of a FAD- and FMN-containing reductase domain, an oxygenase domain that accommodates heme and tetrahydrobiopterin [(6*R*)-5,6,7,8-tetrahydro-L-biopterin, BH4], and a calmodulin binding region. Catalysis takes place at the heme, with the flavins transferring electrons from NADPH to the oxygenase domain. Interdomain electron transfer is strictly dependent on the presence of Ca^{2+}/calmodulin.

The optical absorbance spectrum of NOS exhibits a Soret peak at about 400 nm, originating from a low-spin/high-spin heme mixture (*7*−*9*). In the presence of Arg and BH4 the equilibrium is shifted toward the high-spin state, resulting in a Soret band at about 395 nm (*9*−*13*). This absorbance change can be exploited to determine the equilibrium and kinetic parameters of Arg binding (*10*, *14*). However, because of the large fraction of high-spin heme already present in the absence of Arg, particularly in the physiologically relevant case when BH4 is bound to the enzyme, the corresponding absorbance changes are uncomfortably small. Much larger absorbance changes can be observed, and, consequently, a more accurate determination of the binding parameters achieved, by fully converting the enzyme to a low-spin state prior to titration with Arg. Imidazole forms a low-spin complex with the NOS heme that displays a Soret maximum at 428 nm (*10*, *15*, *16*), and in several studies the conversion of this complex to the high-spin species in the presence of Arg has been recorded to calculate the equilibrium and kinetic binding parameters of Arg (*10*, *16*−*20*). However, divergent results have been reported concerning the interdependence of the binding properties of Arg and imidazole. Some studies reported competitive binding (*18*, *19*), while others found no effect of imidazole on Arg binding to nNOS (*10*, *20*). Likewise, conflicting observations have been made regarding inhibition of NOS by imidazole, for which Arg-competitive (*18*, *21*, *22*) and noncompetitive (*23*, *24*) patterns have been reported.

In this study we investigated the interdependence of binding of Arg, imidazole, and BH4 to recombinant rat brain nNOS, the isoform for which most paradoxical observations have been reported. We found strong competition between Arg and imidazole binding, but not to the extent that formation of a ternary complex is completely prohibited. Since imidazole is still bound to the heme in the ternary complex, titration of Arg in the presence of imidazole does not result in 100% formation of the high-spin state. In

† This work was supported by Grants P 13013-MED, P 13586-MED, and P 14777-GEN of the Fonds zur Förderung der Wissenschaftlichen Forschung in Österreich and by the Human Frontier Science Program (RGP0026/2001-M).

* To whom correspondence should be addressed. Telephone: 43-316-380-5569. Fax: 43-316-380-9890. E-mail: antonius.gorren@kfunigraz.ac.at.

[1] Abbreviations: NOS, nitric oxide synthase; nNOS, eNOS, and iNOS, neuronal, endothelial, and inducible isoforms of NOS; BH4, tetrahydrobiopterin [(6*R*)-5,6,7,8-tetrahydro-6-(L-*erythro*-1′,2′-dihydroxypropyl)pterin]; nNOS(BH4−), BH4-deficient nNOS; nNOS(BH4+), nNOS as isolated, containing 1 equiv of BH4 per dimer.

10.1021/bi025675o CCC: $22.00
Published on Web 05/23/2002

addition, a small fraction (≤10%) bound Arg with low affinity (K_d^{app} in the order of 10^{-3} M). We suggest that these phenomena are the main cause for the contradictory results reported in the literature.

EXPERIMENTAL PROCEDURES

Materials. Recombinant rat brain nNOS was purified from baculovirus-infected Sf9 cells (*25*, *26*). BH4-deficient nNOS was obtained from Sf9 cells infected in the presence of 2,4-diamino-6-hydroxypyrimidine (*27*). BH4 was obtained from Dr. B. Schircks Laboratories (Jona, Switzerland). L-Arginine, imidazole, and other chemicals were from Sigma (Vienna, Austria). Stock solutions of Arg and imidazole (1 M each) were prepared in 50 mM KP_i (pH 7.5) and adjusted to pH 7.5. Throughout this paper the terms nNOS(BH4−) and nNOS(BH4+) refer to the enzyme with ≤0.1 and approximately 1 equiv of BH4 per NOS dimer, respectively (*11*).

UV/Vis Spectroscopy: Equilibrium Titrations. Absorbance spectroscopic titrations were carried out at ambient temperature with a Hewlett-Packard 8452A diode array spectrophotometer. The enzyme was diluted to a concentration of 1.5−3.0 μM in 250 μL of 50 mM KP_i (pH 7.5), 0.2 mM CHAPS, 0.5 mM EDTA, and 2.4 mM 2-mercaptoethanol. Arg, imidazole, and BH4 were present as indicated. Absorption spectra were measured between 350 and 820 nm. Arg (or imidazole) was added in small increments by addition of 1.0−7.5 μL aliquots of appropriate dilutions of the 1 M stock solutions. Spectra were measured 2 min after each addition. To correct for increased turbidity in the course of the titrations, straight lines were fitted through the spectra between 720 and 820 nm, where the absorbance of NOS is negligibly small. These lines, extrapolated over the whole spectral range, were subtracted from the raw spectra. These spectra were corrected for the cumulative increase in volume, which was small for each individual addition (≤3%) but usually amounted to about 20% at the end of the titration. This procedure resulted in series of drift-corrected spectra with stable isosbestic points (see Figure 1). Concentrations of the titrating agents were also corrected for the change in volume.

To construct titration curves, absorbance difference spectra were obtained by subtraction of the initial spectrum. The peak-minus-trough amplitude in the Soret region of the difference spectra was then plotted as a function of the concentration of the titrating agent.

In the course of this study we noticed that titrations with Arg in the presence of imidazole did not yield 100% high-spin heme. For this reason we converted the absorbance changes to shifts in the spin-state populations. To derive magnitudes of high-spin heme fractions from the absorption spectra, absorbances at 390 and 430 nm were determined in the presence of 0.1 M Arg (100% high-spin; ref *28*) and in the presence of 0.1 M imidazole (100% imidazole complex; refs *29* and *30*) for each of the investigated NOS preparations. The high-spin fraction for each measured spectrum was then calculated by application of eq 1, in which f_{hs} is the high-spin fraction, R_{obs} is A_{390}/A_{430} (the ratio of the absorbances observed at 390 and 430 nm for each point on the titration curve), R_1 is $A_{390}^{ls}/A_{430}^{ls}$, the corresponding ratio for the imidazole complex, R_2 is $A_{390}^{hs}/A_{430}^{hs}$, the corresponding ratio for the high-spin state, and R_3 is $A_{430}^{hs}/A_{430}^{ls}$. Despite the different methods by which the two series of titration curves were derived, both yielded similar values for the apparent dissociation constants and for the relative amplitudes of high- and low-affinity phases.

$$f_{hs} = \frac{R_1 - R_{obs}}{(R_{obs} - R_2)R_3 - R_{obs} + R_1} \quad (1)$$

It should be noted that this method for calculating high-spin fractions assumes the presence of only two heme species: the high-spin compound and the imidazole complex. This is valid for most titrations reported here but causes an overestimation of the high-spin fraction for the imidazole titrations with nNOS(BH4−) in the absence of Arg and BH4 (cf. Figure 2B) because of a sizable fraction of additional low-spin species initially present under those conditions (*31*). From an analysis of the initial spectra with a previously published procedure (*31*), we estimate that for those titrations the calculated high-spin fraction is too high by 10−20%. The apparent dissociation constants and the relative amplitudes of high- and low-affinity phases are not affected.

All titration curves were first fitted to eq 2, in which f_{hs}^{∞} is the high-spin fraction at saturating concentrations of the titrating agent, Δf_{hs} is the maximal change in high-spin fraction induced by the titration, c is the concentration of the titrating agent, EC_{50} is the concentration of the titrating agent that causes a half-maximal effect, and h is the Hill coefficient. Titration curves yielding Hill coefficients close to 1 were fitted to an empirical equation for monophasic binding (eq 3). All titration curves were also fitted to an empirical equation describing biphasic binding (eq 4), in which f_{hs}^{0} is the high-spin fraction at the start of the titration, Δf_{hs}^{ha} and Δf_{hs}^{la} are the changes in high-spin fraction induced by the high- and low-affinity phases, and K_d^{ha} and K_d^{la} are the corresponding apparent equilibrium dissociation constants. In a few cases, a third phase was introduced (see Results).

$$f_{hs} = f_{hs}^{\infty} - \frac{\Delta f_{hs}}{1 + (c/EC_{50})^h} \quad (2)$$

$$f_{hs} = f_{hs}^{0} + \frac{\Delta f_{hs} c}{K_d + c} \quad (3)$$

$$f_{hs} = f_{hs}^{0} + \frac{\Delta f_{hs}^{ha} c}{K_d^{ha} + c} + \frac{\Delta f_{hs}^{1a} c}{K_d^{1a} + c} \quad (4)$$

All fitting parameters were left free, except in the case of the imidazole titrations at high concentrations of Arg (2.5 and 12.5 mM), shown in Figure 2C. Since these titrations were far from complete at the highest applied concentrations of imidazole, f_{hs}^{∞}, $f_{hs}^{0} + \Delta f_{hs}$, and $f_{hs}^{0} + \Delta f_{hs}^{ha} + \Delta f_{hs}^{la}$ were arbitrarily set to 0. Values of parameters derived from fits are presented together with the error estimated from the fits. Averages of multiple independent determinations are presented ± SEM.

Rapid-Scan/Stopped-Flow Spectroscopy: Kinetics of Arg Binding. Rapid-scan spectra were measured with a Bio-Sequential SX-17MV stopped-flow ASVD spectrofluorometer (Applied Photophysics, Leatherhead, U.K.). Samples

Table 1: Fitting Parameters for Titrations of nNOS with Imidazole[a]

BH4[b] endog (μM)	BH4[b] exog (μM)	Arg (mM)	f_{hs}^0	Δf_{hs}^{ha}	K_d^{ha} (μM)	Δf_{hs}^{la}	K_d^{la} (mM)	n
−	−	−	0.81 ± 0.05	0.65 ± 0.01	48 ± 7	0.14 ± 0.06	10 ± 8	3
+	−	−	0.86 ± 0.05	0.62 ± 0.13	73 ± 11	0.19 ± 0.09	1.7 ± 0.5	4
+	10	−	0.87 ± 0.04	0.79 ± 0.13	192 ± 44	0.10 ± 0.07	3.9 ± 1.4	4
+	−	0.1	0.95 ± 0.03	0.30 ± 0.04	141 ± 18	0.63 ± 0.05	16 ± 3	4
+	10	0.1	0.93 ± 0.04	0.14 ± 0.03	46 ± 7	0.74 ± 0.02	19 ± 2	5

[a] Titrations of nNOS(BH4−) and nNOS(BH4+) in the presence of varying concentrations of BH4 and Arg were fitted biphasically (eq 4). Parameters are presented as averages of n independent determinations ± SEM. See Experimental Procedures for further details. [b] Experiments were carried out with nNOS(BH4−) or nNOS(BH4+), designated in the first column by (−) and (+), respectively, and in the absence or presence of 10 μM exogenous BH4, as indicated in the second column; endog, endogenous; exog, exogenous.

were illuminated with an ozone-free 150 W xenon lamp and detected with a photodiode array, equipped with a 200−730 nm grating. Series of spectra were acquired over total reaction times varying between 0.1 and 1000 s. The reaction was started by rapid mixing of nNOS (final concentration after mixing 1−2 μM) with varying concentrations of Arg. Both syringes contained 50 mM KP_i (pH 7.5), 0.2 mM CHAPS, 0.5 mM EDTA, 2.4 mM 2-mercaptoethanol, and BH4 and imidazole as indicated. Reactions were performed at 15 °C.

To construct kinetic traces, absorbance difference spectra were obtained by subtracting the initial spectrum. The two wavelengths that yielded the largest positive and negative absorbance changes were selected, and the absorbance differences between these two wavelengths (387 and 419 nm in the absence and 385 and 428 nm in the presence of imidazole) for each spectrum were plotted as a function of time. This procedure yielded an optimal signal-to-noise ratio and largely eliminated apparent absorbance changes caused by random drift. The signal-to-noise ratio of the kinetic traces was further improved by application of a five-point moving average smoothing procedure.

All traces were fit to single exponentials or, when appropriate, to a combination of two exponentials according to eqs 5 and 6, in which ΔA_0 is the absorbance difference between the selected wavelengths in the spectrum at time zero, $\Delta\Delta A$, $\Delta\Delta A_1$, and $\Delta\Delta A_2$ are the changes in the amplitude of the absorbance difference, and k, k_1, and k_2 are the observed first-order rate constants.

$$\Delta A(t) = \Delta A_0 + \Delta\Delta A(1 - e^{-kt}) \quad (5)$$

$$\Delta A(t) = \Delta A_0 + \Delta\Delta A_1(1 - e^{-k_1 t}) + \Delta\Delta A_2(1 - e^{-k_2 t}) \quad (6)$$

Values of parameters derived from fits are presented together with the error estimated from the fits. Averages of multiple independent determinations are presented ± SEM.

RESULTS

Absorbance Spectral Changes for nNOS in the Presence of Imidazole and Arg. As isolated, the heme of nNOS(BH4+) was largely in the high-spin state (85−95%), exhibiting a Soret peak at 396 nm. When this enzyme species was titrated with imidazole, formation of the low-spin ferric heme−imidazole complex resulted in a shift of the Soret peak to 428 nm (Figure 1A). Conversely, titration of the imidazole complex with Arg shifted the spectrum back toward high spin (λ_{max} 398 nm; Figure 1B). Most significantly, however, in the presence of 1 mM imidazole the low-spin complex of nNOS(BH4+) could not be completely reverted to the high-spin state by addition of arginine, even though the low-spin complex was not fully formed at 1 mM imidazole (Figure 1B). In the absence of imidazole both nNOS(BH4+) and nNOS(BH4−) were readily converted to 100% high spin in the presence of Arg (not shown). Therefore, the incomplete formation of the high-spin species is not due to a deficiency of the enzyme in arginine binding.

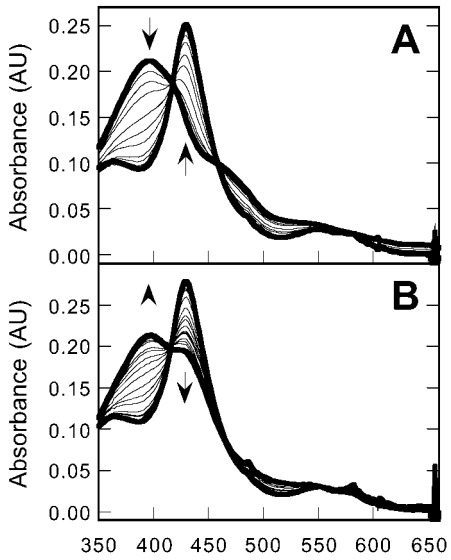

FIGURE 1: Absorption spectra of nNOS(BH4+) in the presence of various concentrations of Arg and imidazole. Panel A shows the spectral changes induced by the addition of increasing concentratons (0−0.15 M) of imidazole to 3 μM nNOS(BH4+). Panel B shows the spectral changes induced by the addition of increasing concentrations (0−0.14 M) of Arg to 3 μM nNOS(BH4+) in the presence of 1 mM imidazole. In both panels the direction of the absorbance changes is indicated by arrows. Thick lines mark the first and last spectra of each series. Experimental conditions: 50 mM KP_i (pH 7.5), 0.2 mM CHAPS, 0.5 mM EDTA, 2.4 mM 2-mercaptoethanol, and ambient temperature. For further details see Experimental Procedures.

Titrations of nNOS with Imidazole. Titration curves corresponding to formation of the low-spin ferric heme−imidazole complex with nNOS(BH4+) (Figure 2A) were almost monophasic and could be satisfactorily fitted to a single-site binding model (K_d^{app} of 153 ± 46 μM, $n = 3$; not shown). A slight improvement was achieved by introduction of a second phase (fit shown in Figure 2A), with the majority of sites (77%) binding imidazole with a K_d^{app} of 73 ± 11 μM and a minor fraction exhibiting lower affinity (K_d^{app} ~ 1.7 ± 0.5 mM, $n = 4$; Table 1).

A possible source of heterogeneous binding is the presence of only 1 equiv of BH4 per heme in the enzyme as isolated. Titration in the presence of a saturating concentration of BH4

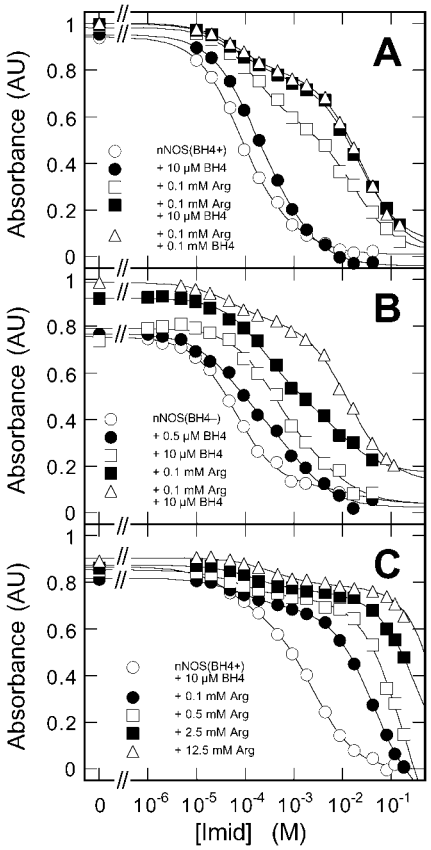

FIGURE 2: Titration of nNOS with imidazole. Panel A shows titration curves of 3 μM nNOS(BH4+) in the absence of Arg and exogenous BH4 (open circles) and in the presence of 10 μM BH4 (closed circles), 0.1 mM Arg (open squares), 0.1 mM Arg + 10 μM BH4 (closed squares), and 0.1 mM Arg + 0.1 mM BH4 (open triangles). Panel B illustrates the effect of BH4 on the titration of 1 μM nNOS(BH4−) with imidazole. Shown are titration curves in the absence of BH4 (open circles), 0.5 μM BH4 (a half-saturating concentration, closed circles), 10 μM BH4 (open squares), 0.1 mM Arg (closed squares), and 0.1 mM Arg + 10 μM BH4 (open triangles). Panel C illustrates the effect of the concentration of Arg on the titration of 3 μM nNOS(BH4+) with imidazole. Shown are titrations in the presence of 10 μM BH4 and 0 (open circles), 0.1 (closed circles), 0.5 (open squares), 2.5 (closed squares), and 12.5 mM Arg (open triangles). Other experimental conditions were as in Figure 1. The lines drawn through the data points are best fits to a biphasic binding model as described in Experimental Procedures. See Results for further details.

(10 μM) resulted in a slightly right-shifted curve (Figure 2A), with monophasic fitting yielding a K_d^{app} of 0.33 ± 0.14 mM (n = 3; not shown). However, exogenous BH4 did not completely eliminate the slight heterogeneity in imidazole binding, and an improved fit was again obtained by introduction of a minor low-affinity phase (fit shown in Figure 2A; average fitting parameters shown in Table 1). Higher concentrations of BH4 (0.1 mM) did not affect the imidazole binding curve any further (not shown). The impairment of imidazole binding by BH4 was more conspicuous in titrations with BH4-deficient nNOS (Figure 2B), because the very low BH4 content of this enzyme species resulted in a lower high-affinity K_d^{app} compared to nNOS(BH4+) (48 ± 7 μM, n = 3; Table 1), while the values of K_d^{app} for nNOS(BH4−) and nNOS(BH4+) in the presence of 10 μM BH4 were similar. For the titrations shown in Figure 2B, exogenous BH4 induced a 6-fold increase of the high-affinity K_d^{app} from 61 ± 5 μM to 0.36 ± 0.14 mM. Titration of BH4-deficient nNOS with imidazole in the presence of a half-saturating concentration of BH4 yielded a distinctly biphasic curve, in line with expectation (Figure 2B).

Arginine (100 μM) caused a rightward shift of the titration curves of nNOS(BH4+) (Figure 2A) and nNOS(BH4−) (Figure 2B), and imidazole binding became strongly biphasic. Biphasic fitting indicated that a substantial fraction of the enzyme exhibited a similar apparent affinity for imidazole as in the absence of Arg (K_d^{app} of 141 ± 18 μM, n = 4; Table 1), but the major fraction now bound imidazole with much lower affinity (K_d^{app} of 16 ± 3 mM; Table 1). When the same experiments were performed in the presence of 10 μM BH4, the titration curves shifted further rightward (Figure 2A,B), which was due to a decrease in the contribution of the high-affinity phase (Table 1). However, a small fraction (16 ± 3% of the total change) still bound imidazole with an affinity similar to that of nNOS(BH4−) in the absence of Arg (Table 1). Increasing the concentration of BH4 to 0.1 mM did not induce any further changes in the titration curves (Figure 2A).

In the presence of higher concentrations of Arg, titration curves of imidazole binding to BH4-saturated nNOS were shifted further rightward (Figure 2C). While increasing the concentration of Arg did not affect the relative contributions of the high- and low-affinity binding phases, it raised the low-affinity K_d^{app} of imidazole and, at concentrations above 0.5 mM, the high-affinity K_d^{app} as well (Figure 3). In the case of mutually exclusive binding of Arg and imidazole, a linear relationship between the observed imidazole dissociation constant and [Arg] is expected:

$$K_d^{obs}(\mathrm{Im}) = K_d(\mathrm{Im})\left(1 + \frac{[\mathrm{Arg}]}{K_d(\mathrm{Arg})}\right) \qquad (7a)$$

For the apparent high-affinity imidazole binding phase (which corresponds to low-affinity binding of Arg!) we obtained 2.3 ± 0.9 mM for K_d(Arg) and 52 ± 12 μM for K_d(Im) from fits of the data in Figure 3 to eq 7a. For the apparent high-affinity dissociation constant of arginine we obtained a value of 1.26 ± 0.10 μM, by fitting the linear part of the curve corresponding to low-affinity imidazole binding (dotted line in Figure 3) to eq 7a and assuming a value of 0.2 mM for K_d(Im) in the presence of BH4 (Table 1).

At high concentrations of Arg, the plot of the observed low-affinity imidazole binding constant deviated from linearity, suggesting that the inhibitory effect of Arg on imidazole binding is saturable and that a ternary complex is formed at very high concentrations of Arg and imidazole. It should be noted, however, that formation of the imidazole complex was far from complete at the end of those titrations, obtained in the presence of 2.5 and 12.5 mM Arg, that exhibited the largest deviation from linearity (see Figure 2C).

Titrations of nNOS with Arginine. As was illustrated above (see Figure 1B), the low-spin imidazole complex of nNOS(BH4+), induced by 1 mM imidazole, could not be completely reverted to high spin by addition of arginine, even though formation of the low-spin complex was not complete at a concentration of 1 mM imidazole. We obtained maximal high-spin levels of 76 ± 3% (n = 5) and 83 ± 2% (n = 5) in the absence and presence of 10 μM BH4, respectively. Higher concentrations of BH4 did not increase the high-spin

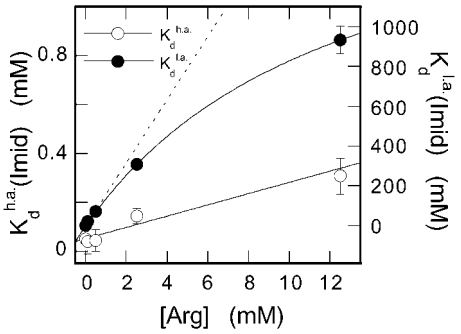

FIGURE 3: Dependence of the apparent dissociation constants of imidazole on the concentration of Arg. Apparent high- and low-affinity dissociation constants for binding of imidazole to nNOS-(BH4+) in the presence of 10 μM BH4 were derived from the biphasic titration curves in Figure 2C and plotted as a function of the concentration of Arg. The high-affinity phase (open circles), corresponding to 10−12% of imidazole binding, was only weakly affected by Arg. Most imidazole binding was, however, strongly inhibited by Arg, resulting in a low-affinity phase (closed circles; please note the difference of 3 orders of magnitude in vertical scaling). See Results for further details. The straight line through the data points of the apparent high-affinity K_d is the best fit to eq 7a. The straight dotted line through the first three data points for the low-affinity K_d, is the best fit to eq 7a assuming a value of 0.2 mM for K_d(Im). The curved line illustrates the deviation of the apparent low-affinity dissociation constant from linearity at high concentrations of Arg and is a best fit to eq 10, assuming a value of 0.2 mM for K_d(Im). Equation 10 describes the behavior expected for the observed apparent dissociation constant [K_d(obs)] in the case of anticooperative binding of Arg and imidazole, with K_d(Arg) representing the K_d for arginine in the absence of imidazole, and K_d(Im) and K_d'(Im) representing the K_d for imidazole in the absence and presence of Arg, respectively. Optimal fitting parameters were 1.4 ± 0.3 μM for K_d(Arg) and 1.89 ± 0.05 M for K_d'(Im), yielding a value for the K_d for Arg in the presence of imidazole [K_d'(Arg)] of 13 ± 3 mM.

$$K_d^{obs} = \frac{K_d(\mathrm{Arg}) + [\mathrm{Arg}]}{K_d(\mathrm{Arg})/K_d(\mathrm{Im}) + [\mathrm{Arg}]/K_d'(\mathrm{Im})} \qquad (10)$$

yield any further (not shown). Typical arginine titration curves of nNOS(BH4+) in the presence of 1−100 mM imidazole are shown in Figure 4. Without BH4 and in the presence of 1 mM imidazole, the initial high-spin fraction (30%) increased to 80% but did not rise above that level (Figure 4A). The titrations exhibited several poorly resolved phases, resulting in unusually flat curves. A satisfactory fit required at least three phases ($f_0 = 0.28 \pm 0.07$, $\Delta f_1 = 0.21 \pm 0.05$, $K_{d1} = 4.2 \pm 2.4$ μM, $\Delta f_2 = 0.14 \pm 0.04$, $K_{d2} = 98 \pm 31$ μM, $\Delta f_3 = 0.17 \pm 0.01$, $K_{d3} = 20 \pm 4$ mM, $n = 6$, with the suffixes 1, 2, and 3 corresponding to the three phases). In the presence of 10 μM BH4 the initial and final high-spin fractions were greater, but the anomalous appearance of the titration curve persisted (Figure 4B; fitting parameters $f_0 = 0.43 \pm 0.07$, $\Delta f_1 = 0.14 \pm 0.02$, $K_{d1} = 3.0 \pm 0.7$ μM, $\Delta f_2 = 0.19 \pm 0.06$, $K_{d2} = 57 \pm 25$ μM, $\Delta f_3 = 0.18 \pm 0.06$, $K_{d3} = 18 \pm 4$ mM, $n = 6$). Raising the concentration of BH4 to 100 μM did not produce any further changes to the titration curves (not shown).

Increasing the concentration of imidazole from 1 to 10 mM lowered the observed initial and final fractions of high-spin heme in titrations of nNOS(BH4+) with Arg in the absence (Figure 4A) and presence of 10 μM BH4 (Figure 4B). Although still not monophasic, the titration curves became less irregular and could be satisfactorily fitted with

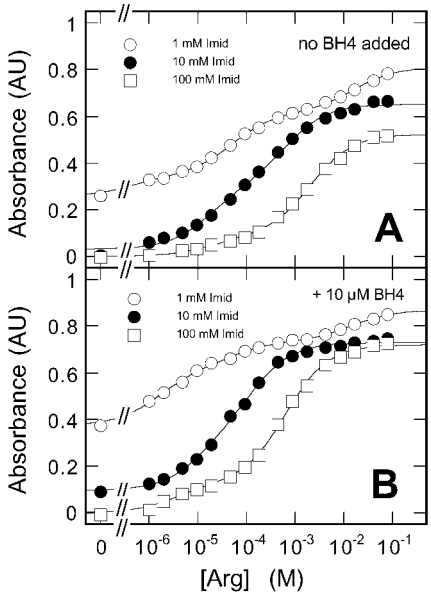

FIGURE 4: Titration of nNOS with Arg. Panels A and B show titration curves of 3 μM nNOS(BH4+) in the absence and presence of 10 μM exogenous BH4, respectively. Titrations were performed in the presence of 1 mM (open circles), 10 mM (closed circles), and 100 mM imidazole (open squares). Other experimental conditions were as in Figure 1. The lines drawn through the data points are best fits to a biphasic binding model as described in Experimental Procedures, except for the titration curves in the presence of 1 mM imidazole, which were fitted with three phases. See Results for further details.

two phases (fitting parameters: $f_{hs}^0 = 0.03 \pm 0.01$, $\Delta f_{hs}^{ha} = 0.27 \pm 0.03$, $K_d^{ha} = 17 \pm 5$ μM, $\Delta f_{hs}^{la} = 0.35 \pm 0.03$, $K_d^{la} = 0.64 \pm 0.15$ mM in the absence of exogenous BH4; $f_{ha}^0 = 0.10 \pm 0.01$, $\Delta f_{hs}^{ha} = 0.25 \pm 0.08$, $K_d^{ha} = 11 \pm 6$ μM, $\Delta f_{hs}^{la} = 0.38 \pm 0.08$, $K_d^{la} = 0.13 \pm 0.04$ mM in the presence of 10 μM BH4).

Fitting the curves obtained with 1 and 10 mM imidazole to a single-site binding model (eq 3) or to the Hill equation (eq 2) yielded very similar apparent K_d and EC_{50} values (not shown), erroneously suggesting that imidazole does not affect the affinity of Arg. However, at a concentration of 100 mM, an inhibitory effect of imidazole on Arg binding became evident, since titration curves were clearly right-shifted with respect to those obtained with 10 mM imidazole (Figure 4). When curves obtained with 10 and 100 mM imidazole were fitted to the Hill equation, increasing the imidazole concentration resulted in a 10-fold increase of the EC_{50} values, from 0.148 ± 0.007 to 1.71 ± 0.02 mM in the absence and from 0.052 ± 0.003 to 0.46 ± 0.06 mM in the presence of 10 μM BH4. Moreover, the maximally attained high-spin fraction decreased with increasing imidazole concentrations, particularly in the absence of exogenous BH4 (Figure 4). The right shift is due to a decrease of the contribution of the high-affinity phase and an increase in K_d^{app} of the low-affinity phase (fitting parameters: $f_{hs}^0 = 0.00 \pm 0.01$, $\Delta f_{hs}^{ha} = 0.09 \pm 0.01$, $K_d^{ha} = 19 \pm 9$ μM, $\Delta f_{hs}^{la} = 0.44 \pm 0.01$, $K_d^{la} = 2.0 \pm 0.2$ mM in the absence of exogenous BH4; $f_{hs}^0 = 0.00 \pm 0.01$, $\Delta f_{hs}^{ha} = 0.13 \pm 0.01$, $K_d^{ha} = 4 \pm 1$ μM, $\Delta f_{hs}^{la} = 0.59 \pm 0.01$, $K_d^{la} = 0.63 \pm 0.04$ mM in the presence of 10 μM BH4). Consequently, at 100 mM imidazole approximately 83% of the absorbance change takes place in an imidazole-dependent low-affinity phase. From the corresponding ap-

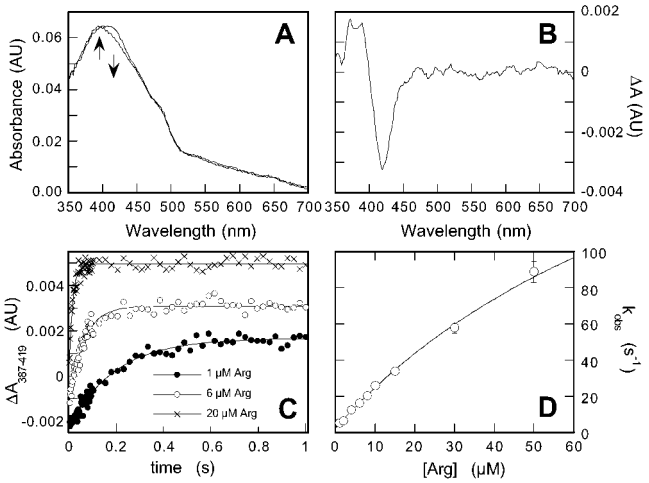

FIGURE 5: Association kinetics of Arg to nNOS(BH4+) in the absence of imidazole. Panel A shows the absorbance spectra observed 2 ms and 1 s after the addition of 10 μM Arg to 1 μM nNOS(BH4+). To account for random drift, the spectra were arbitrarily set equal at 730 nm. The arrows indicate the direction of the absorbance changes. Panel B shows the corresponding absorbance difference spectrum. The signal-to-noise ratio in the absorbance difference spectrum was improved by a five-point moving average smoothing procedure. Panel C shows representative kinetic traces, derived from series of rapid-scan spectra as elaborated in Experimental Procedures. Shown are the binding kinetics at 1 μM (closed circles), 6 μM (open circles), and 20 μM Arg (crosses). The lines through the data points are best fits to single exponentials. For the sake of clarity, the traces obtained at 6 and 20 μM Arg have been vertically offset by +0.001 and +0.002, respectively. Panel D shows the observed pseudo-first-order rate constants as a function of the concentration of Arg. The line through the data points is the best fit to eq 8. See Results for further details. Experimental conditions: 1 μM nNOS(BH4+), 50 mM KP_i (pH 7.5), 0.2 mM CHAPS, 0.5 mM EDTA, 2.4 mM 2-mercaptoethanol, 1−50 μM Arg, and 15 °C.

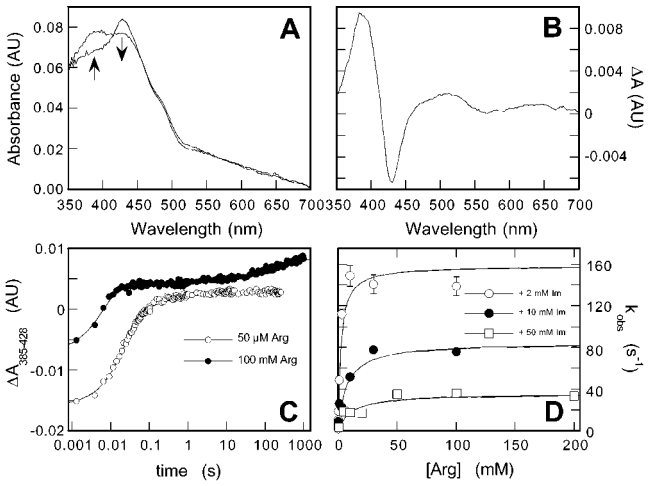

FIGURE 6: Association kinetics of Arg to nNOS(BH4+) in the presence of imidazole. Panel A shows the absorbance spectra observed 2 ms and 1 s after the addition of 50 μM Arg to 1.5 μM nNOS(BH4+) in the presence of 1 mM imidazole. To account for random drift, the spectra were arbitrarily set equal at 730 nm. The arrows indicate the direction of the absorbance changes. Panel B shows the corresponding absorbance difference spectrum. The signal-to-noise ratio in the absorbance difference spectrum was improved by a five-point moving average smoothing procedure. Panel C shows representative kinetic traces, derived from series of rapid-scan spectra as elaborated in Experimental Procedures. Shown are the binding kinetics at 50 μM (open circles) and 100 mM Arg (closed circles) in the presence of 1 mM imidazole. The lines through the data points are best fits to double exponential binding kinetics. For the sake of clarity, the trace obtained at 100 mM Arg has been vertically offset by +0.02. The reaction time is presented logarithmically to facilitate visualization of both kinetic phases. Panel D shows the observed pseudo-first-order rate constants as a function of the concentration of Arg in the presence of 2 mM (open circles), 10 mM (closed circles), and 50 mM imidazole (open squares). The lines through the data points are best fits to eq 8. See Results for further details. Experimental conditions: 1.5 μM nNOS(BH4+), 50 mM KP_i (pH 7.5), 0.2 mM CHAPS, 0.5 mM EDTA, 2.4 mM 2-mercaptoethanol, 10 μM to 200 mM Arg, imidazole as indicated, and 15 °C.

parent dissociation constants (2.0 and 0.63 mM in the absence and presence of BH4, respectively), and assuming values for K_d(Im) of 0.07 and 0.2 mM in the absence and presence of BH4, respectively (Table 1), we estimated values for K_d-(Arg) of 1.24 ± 0.08 and 1.40 ± 0.14 μM by application of eq 7b, in good agreement with the value derived from the titrations with imidazole.

$$K_d^{obs}(\text{Arg}) = K_d(\text{Arg})\left(1 + \frac{[\text{Im}]}{K_d(\text{Im})}\right) \qquad (7b)$$

Rapid-Scan/Stopped-Flow Studies of Arg Binding to nNOS. The small fraction (≤15%) of low-spin heme, present in nNOS(BH4+), renders difficult, but not impossible, the direct determination of Arg binding to this enzyme species. Figure 5A illustrates the small absorbance changes accompanying binding of Arg to nNOS(BH4+). The corresponding difference spectrum is shown in Figure 5B. Examples of kinetic traces, obtained at three different concentrations of Arg, are presented in Figure 5C. These traces were well-fitted to single exponentials (Figure 5C). In Figure 5D the dependence of the observed pseudo-first-order rate constants on the concentration of Arg is plotted. The obtained curve was satisfactorily fitted to the empirical equation shown in eq 8, in which k_a' and k_d' represent apparent rate constants for association and dissociation of Arg and k_{max} (or rather $k_{max} + k_d'$) is the limiting rate constant at saturating concentrations of Arg. The physical meaning of the apparent rate constants

$$k_{obs} = \frac{k_{max}[\text{Arg}]}{k_{max}/k_a' + [\text{Arg}]} + k_d' \qquad (8)$$

depends on the underlying mechanism (see Discussion). The values we derived for the apparent rate constants were (2.5 ± 0.1) × 10^6 $M^{-1}\cdot s^{-1}$ for k_a', 2.5 ± 0.3 s^{-1} for k_d', and 265 ± 63 s^{-1} for k_{max}. Experiments with another batch of protein yielded similar results (not shown).

The same experimental protocol was applied to study the binding of Arg to nNOS(BH4+) in the presence of imidazole. Panels A and B of Figure 6 show absolute and difference spectra obtained with 50 μM Arg in the presence of 1 mM imidazole as an example. As observed in the equilibrium titration studies (cf. Figure 1B), complete formation of the high-spin state did not occur, even in the presence of subsaturating concentrations of imidazole (Figure 6A) and at Arg concentrations of up to 200 mM (not shown). The binding kinetics in the presence of imidazole were monophasic at low concentrations of Arg, with most of the reaction occurring within the first 100 ms, but at high Arg concentrations a slow component, taking place on a time scale of

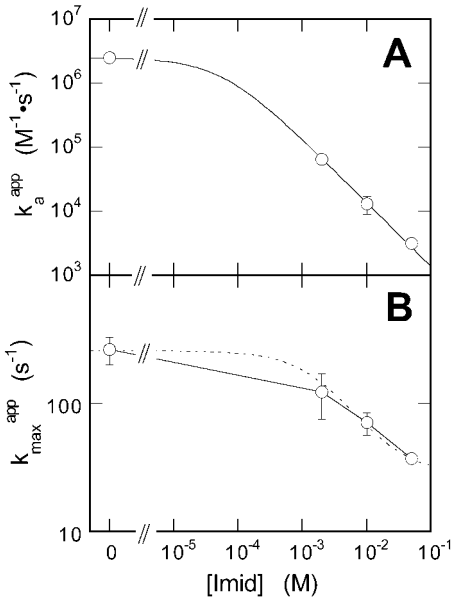

FIGURE 7: Dependence of the apparent kinetic parameters for Arg binding on the imidazole concentration. Values for the apparent association rate constant for Arg binding to nNOS(BH4+) (k_a^{app}, panel A) and for the apparent maximal rate constant of Arg binding (k_{max}^{app}, panel B) in the absence and presence of imidazole were derived from the fits shown in Figures 5D and 6D and plotted against the imidazole concentration. The line drawn through the data points in panel A is the best fit to eq 9; the dotted line drawn through the data points in panel B is the best fit to the equation $k_{max}^{app} = (k_{max}^{0} - k_{max}^{\infty})K_d(\mathrm{Im})/([\mathrm{Im}] + K_d(\mathrm{Im})) + k_{max}^{\infty}$, with k_{max}^{0} and k_{max}^{∞} representing the maximal rate constants in the absence and presence of imidazole, respectively. See Results for details.

Scheme 1

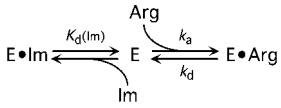

minutes, became apparent (Figure 6C). In Figure 6D the [Arg] dependence of the observed first-order rate constants of the fast phase is shown for three different concentrations of imidazole. As in the absence of imidazole, the observations could be fitted to a hyperbola (eq 8), which revealed that with increasing concentrations of imidazole the apparent rate of association of Arg (k_a') became slower, reaching a value of $(3.2 \pm 0.4) \times 10^3$ $M^{-1}\cdot s^{-1}$ in the presence of 50 mM imidazole (Figure 7A). Concomitantly, the rate constant corresponding to the upper limit (k_{max}) decreased to 37 ± 2 s^{-1} (Figure 7B). The experimental error in the third fitting parameter (k_d') was too large to allow proper assessment.

In the case of simple competition between imidazole and Arg for binding to NOS according to Scheme 1, the apparent second-order association rate constant of Arg will depend on the concentration of imidazole according to eq 9, in which k_a is the second-order Arg association rate constant, K_d(Im) is the equilibrium dissociation constant for imidazole, and [Im] is the imidazole concentration. When we fitted the

$$k_a^{app} = \frac{k_a}{[\mathrm{Im}]/K_d(\mathrm{Im}) + 1} \quad (9)$$

observed rate constants in the absence and presence of imidazole, derived from Figures 5D and 6D, respectively, to this equation (Figure 7A), we obtained values of 2.5×10^6 $M^{-1}\cdot s^{-1}$ for k_a and of 55 ± 4 μM for K_d(Im). The latter value is in excellent agreement with the dissociation constant derived from equilibrium titrations (Figure 2 and Table 1).

Scheme 2

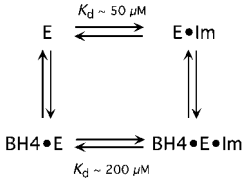

The slow phase of Arg binding was hardly discernible at low concentrations of Arg but became more prominent at Arg concentrations of 10 mM and higher. The rate of this phase, which involved less than 10% of the enzyme, appeared not to be affected by the concentration of Arg or imidazole. We obtained a rate constant of 0.017 ± 0.003 s^{-1} ($n = 7$; pooled observations at different concentrations of Arg and imidazole), similar to the value of 0.2−0.6 min^{-1} that we previously reported for binding of Arg and BH4 to nNOS(BH4−) (*11*).

DISCUSSION

Imidazole inhibits all NOS isoforms (*21*−*24*), but divergent results have been reported with respect to the type of inhibition. Whereas some studies found inhibition by imidazole to be competitive with Arg, in other instances no competition was observed (Table 2). Imidazole binds to the heme and inhibits activity by preventing heme reduction and/or oxygen binding. Consequently, different inhibitory patterns might be accommodated, depending on the steric constraints of the active site pocket, which may vary in a species- and isoform-specific fashion.

The first study on the conversion by Arg of the 428 nm imidazole complex of nNOS to the 395 nm high-spin state reported that the K_d^{app} for Arg was not affected by imidazole (*10*), seemingly in agreement with the lack of competition between Arg and imidazole in inhibition studies (*23*). However, the absence of an effect of imidazole on Arg binding in UV/vis optical spectroscopy is problematic. In these experiments Arg binding is monitored by measuring the absorbance changes that accompany the expulsion of imidazole from its binding site on the heme. As this implies that Arg obstructs imidazole binding, the reciprocal effect is expected as well. Indeed, several later studies in which this method was used to determine the equilibrium dissociation constant of Arg presupposed or found such interactions (*16*−*19*, *32*). The results reported here shed light on the origins of the apparent discrepancies in the literature.

BH4 Impedes but Does Not Prevent Imidazole Binding to nNOS. We calculated a K_d of 0.05 mM for binding of imidazole to nNOS(BH4−), 3−4 times lower than reported values for nNOS (Table 2). Previous studies with nNOS were carried out with BH4-containing enzyme, which explains the slightly higher K_d values. Accordingly, we found that K_d(Im) was increased by 10 μM BH4 to 0.2 mM. The effect of BH4 was saturable, with no further increase of K_d(Im) in the presence of 100 μM BH4. This demonstrates that nNOS can accommodate BH4 and imidazole simultaneously (Scheme 2).

Several prior studies found no effect of BH4 on imidazole binding and inhibition (Table 2). Again, endogenous BH4

Table 2: Published Data on the Interactions of NOS with Imidazole

isoform	source[a]	expression system[a]	IC_{50} (μM)	K_d^{app} (μM)	Arg-competitive	BH4-competitive	ref
nNOS	bovine brain		200		no		*23*
nNOS	GH3 cells					no	*23*
nNOS	rat brain	HEK 293		160	no[b]		*10*
nNOS	porcine brain		390	198[c]	yes	no	*21*
nNOS	rat brain	*E. coli*			yes[d]		*17*
nNOS	human	baculovirus/Sf9	175				*18*
nNOS	rat brain	HEK 293			no		*20*
iNOS	RAW 264.7		40		no	no	*24*
iNOS	hu hepatoc	baculovirus/Sf9	59	63	yes		*18*
iNOS	hu hepatoc	NIH 3T3				yes	*18*
iNOS	RAW 264.7		33				*12*
eNOS	bovine		50		yes	no	*22*
$eNOS_{oxy}$	human	baculovirus/Sf9		73	yes[d]		*16*
eNOS	human	baculovirus/Sf9	189				*18*
eNOS	human	baculovirus/Sf9		110	yes		*19*
eNOS	human	baculovirus/Sf9		100	yes		*32*
eNOS	bovine	*E. coli*				no[e]	*32*

[a] GH3 cells, GH3 pituitary adenoma cells; RAW 264.7, a murine macrophage cell line; hu hepatoc, human hepatocytes; HEK 293, a human embryonic kidney cell line; baculovirus/Sf9, baculovirus-infected Sf9 insect (*Spodoptera frugiperda*) cells; NIH 3T3, a murine fibroblast cell line. Only enzyme expressed in *E. coli* and NIH 3T3 can be regarded as BH4 free; all other enzyme preparations contained varying and in most cases undetermined amounts of endogenous BH4. [b] Only 70% high-spin species was formed in the presence of Arg, even though the applied imidazole concentration was nonsaturating (75% heme−imidazole complex at the start of the titration). [c] Determined by competition with radiolabeled L-nitro-*N*-arginine. [d] Competition between imidazole and Arg was not measured but was the underlying assumption for the determination of reasonable K_d(Arg) values. [e] BH4 did affect imidazole binding indirectly by stimulation of Arg binding.

may have obscured the rather small effect of BH4 on K_d-(Im). Two studies with BH4-free enzyme reported minor competition between imidazole and BH4 for iNOS and eNOS (*18*, *32*).

It is remarkable that BH4 affects imidazole binding, as BH4 does not bind at the distal side of the heme (*33*, *34*), but there is a precedent for the phenomenon in the shift of the heme spin state that is induced by pterin binding (*9*, *11*, *13*, *35*). Since crystallographic studies showed that BH4 has little effect on the enzyme structure (*34*, *36*), it is unlikely that these effects are mediated by conformational changes. An alternative explanation that needs serious consideration is that the effect of BH4 on imidazole binding involves the dimer−monomer equilibrium. However, it has been reported that imidazole stimulates dimerization of iNOS (*37*). Since BH4 also stimulates dimerization (*13*, *38*−*41*), a mediating role of the oligomeric state of NOS should result in cooperativity between pterin and imidazole binding, contrary to observations. We suspect that the proximity of the pterin to the heme alters its electronic structure in such a way that the ligand binding properties of the iron are modified. Clearly, more research is required to resolve this issue.

Rat Brain nNOS Is Heterogeneous with Respect to Competition between Arg and Imidazole Binding. In the presence of Arg, titrations of nNOS with imidazole remained biphasic even at saturating concentrations of BH4. Moreover, titrations of the imidazole complex with Arg yielded unusually slow-rising curves that never yielded more than about 75−85% high spin. Incomplete regeneration of the high-spin state upon titration of the imidazole complex of recombinant rat brain nNOS with Arg was already noted in the first study of this type (*10*). This peculiar behavior seems to be isoform-specific. Similar experiments with the oxygenase domain of bovine eNOS expressed in *Escherichia coli* yielded standard single-site titration curves for Arg and imidazole under all conditions, with strict competition between Arg and imidazole (unpublished observations).

Scheme 3

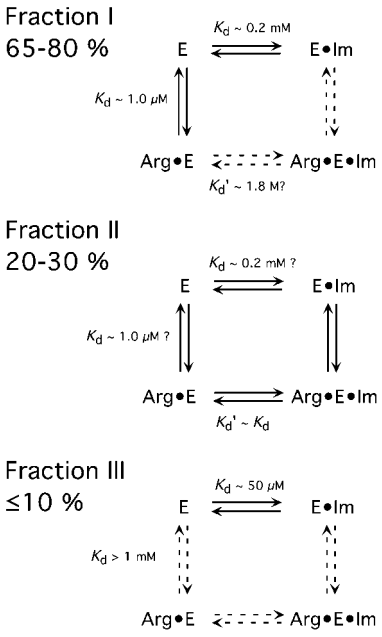

Partly, the anomalous behavior is caused by a minor fraction of nNOS (≤10%) that appears to bind Arg with low affinity (fraction III in Scheme 3). This fraction is reflected in the high-affinity binding phase in titrations with imidazole that was not affected by Arg unless very high concentrations were applied. Fraction III may also be responsible for the slower phase of Arg binding, observed by rapid-scan spectroscopy in the presence of imidazole and high (≥10 mM) concentrations of Arg. Since the size of fraction III was not affected by the concentrations of Arg, imidazole, or BH4, it seems to constitute a distinct population that does not interconvert with the rest of the protein under our experimental conditions.

Although the low affinity for Arg of fraction III partly explains the incomplete high-spin transition in the presence

of high concentrations of imidazole, it is clearly too small to fully account for the magnitude of the NOS fraction that could not be converted to high spin even at nonsaturating levels of imidazole. This suggests that part of the enzyme (20−30%) binds Arg and imidazole in a stable ternary complex (fraction II in Scheme 3). Since the resulting enzyme species is still a six-coordinate heme−imidazole complex, it is expected to have spectral properties identical or very similar to those of the imidazole complex in the absence of Arg, and Arg binding will go unnoticed in optical titrations. In line with this hypothesis, the maximal high-spin level decreased when the imidazole concentration was raised, particularly in the absence of BH4 (Figure 4A). The presence of a nNOS fraction binding Arg and imidazole simultaneously may reconcile the different types of inhibition by imidazole reported previously (Table 2).

The major portion of nNOS (65−80%) showed strong competition between Arg and imidazole (fraction I in Scheme 3). From titrations of nNOS(BH4−) with imidazole in the absence and presence of Arg, we estimate a value of 10−20 μM for K_d(Arg) in the absence of BH4, using eq 7 (results not shown). The physiologically more important value in the presence of BH4 was about 1 μM (calculated from the data shown in Figures 3 and 4). These results imply that the affinity of nNOS for Arg increased in the presence of BH4, in line with the well-documented cooperativity between Arg and pterin binding (*11*, *17*, *40*, *42*). As illustrated by Figure 3, fraction I may also show a tendency to form a ternary complex at extremely high concentrations of the ligands. Scheme 3 illustrates how the various fractions of rat brain nNOS respond to Arg in the presence of imidazole.

Kinetics of Arg Binding. Our data suggest that the determination of the association rate constant of Arg in the presence of imidazole, as has been done in previous studies (*19*, *20*, *32*), may not be straightforward in the case of nNOS. Therefore, we determined the rate of Arg binding directly, in the absence of imidazole. The curve we obtained for the relation between the observed apparent first-order rate constant and the concentration of Arg exhibited a nonzero intercept with the *y*-axis and a hyperbolic increase toward a limiting rate constant. Such behavior is predicted by Scheme 4a, Scheme 4b, or a combination of both. In these models k_1 and k_{-1} are the rate constants for association and dissociation of Arg, and k_2 and k_{-2} are rate constants corresponding to the low-to-high and high-to-low spin-state transition, respectively. The models differ in having Arg binding either preceding or following the spin transition. The parameters that can be derived from Figure 5D have slightly different physical meaning depending on the prevalent pathway. However, it can be deduced that, for the reaction studied here, the apparent rate constants (k_a', k_d', k_{max}) will closely resemble k_1, k_{-1}, and k_2 for either model in first approximation.

We found an association rate constant of (2.5 ± 0.1) × 10^6 $M^{-1}\cdot s^{-1}$, somewhat higher than the rate constants reported for eNOS (2×10^5 and 8×10^5 $M^{-1}\cdot s^{-1}$ at 4 and 23 °C, respectively; ref *19*), which probably represents a true difference between the isoforms. It is also 16 times higher than a value that was obtained for nNOS in the presence of imidazole under the assumption that imidazole did not affect the rate of Arg binding (*20*). As evident from the results reported here, this assumption may have resulted in an underestimation of the rate constant. For the dissociation rate constant we found 2.5 ± 0.3 s^{-1} in fair agreement with both reports (*19*, *20*). For the equilibrium dissociation constant of Arg we derive 1.0 ± 0.2 μM, in confirmation of the optical titrations (see above).

Scheme 4

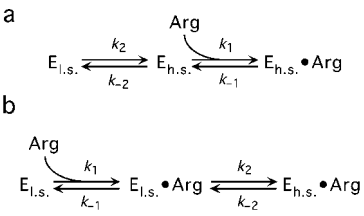

Scheme 5

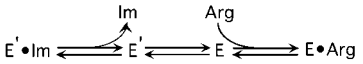

The observation of a limiting first-order rate constant demonstrates that at saturating concentrations of Arg some protein-associated reaction step becomes rate-determining. In Scheme 4 this step is designated as a change of the spin state, but it is likely that the spin-state change is intrinsically fast and diagnostic of an underlying protein conformational change. We made similar observations in previous studies on binding of BH4 and Arg to nNOS(BH4−), except that in that case the conformational change was so slow (0.2−0.6 min^{-1}) that the low-to-high spin transition was not affected by the concentrations of BH4 and Arg (*11*). Since identical rates were found for BH4 and Arg binding in that study, we concluded that the spin-state transition probably preceded Arg/BH4 binding, which corresponds to Scheme 4a. Assuming that the same mechanism is valid for nNOS(BH4−) and nNOS(BH4+), we propose that Scheme 4a describes the kinetics of Arg binding in this study as well.

The corresponding experiments in the presence of imidazole clearly demonstrated competition between Arg and imidazole by a sharp decrease in the apparent association rate constant when the imidazole concentration was raised. The observations were well fitted to a model of simple competition (Scheme 1), yielding a value for K_d(Im) of 55 ± 4 μM, in agreement with the value obtained from equilibrium titrations.

Surprisingly, the limiting rate constant also decreased with higher imidazole concentrations. A simple mechanism accounting for this is furnished by Scheme 5, in which imidazole lowers the apparent limiting rate constant by shifting the equilibrium E′·Im ⇔ E′ to the left. However, fitting the observations to the corresponding equation yielded a dissociation constant of imidazole in the millimolar range, which is inconsistent with the value determined by other methods. Several alternative mechanisms accommodating a declining limiting rate constant also yielded unacceptable values for K_d(Im). X-ray crystallography studies demonstrated the binding of two imidazoles in the active site of the iNOS oxygenase domain (*43*). Possibly, a second imidazole is involved in the decrease of the limiting rate.

General Discussion. Rat brain nNOS behaved heterogeneously with respect to Arg and imidazole binding, with the majority of the protein showing strong competition between Arg and imidazole, but with smaller populations exhibiting little or no competition, binding Arg poorly, or displaying

weak imidazole binding. This may be the cause of most of the conflicting literature on the interactions of nNOS with Arg and imidazole, since the method of choice has been the titration of the imidazole complex with Arg. As the ternary complex with Arg and imidazole exhibits the same spectral properties as the imidazole complex, formation of this species will be observable in a titration with imidazole but not with Arg. As a result, titration curves with Arg may become almost uninterpretable, particularly in the presence of a subsaturating concentration of imidazole (such as 1 mM) and substoichiometric BH4 (such as in nNOS as isolated). The otherwise puzzling observation of an imidazole-independent transformation by Arg of the imidazole complex to the high-spin state may have been a direct consequence. Indeed, under such conditions we also obtained Arg titrations that appeared not to be affected by imidazole, apart from the different initial and final high-spin fractions (cf. the titration curves with 1 and 10 mM imidazole in Figure 4).

The varying reported modes of imidazole binding and inhibition have been interpreted to reflect isoform-specific differences in geometry of the substrate binding pocket, with the available space decreasing in the order nNOS > iNOS > eNOS. From Table 2 it is clear that this is an oversimplification, and the results presented here suggest that some of the reported differences, particularly between isoforms from different sources, may be artifactual. Nevertheless, an isoform-dependent trend is apparent. Specifically, all reports agree that binding of imidazole and Arg is mutually exclusive in eNOS, whereas we suspect that the heterogeneity described here, with part of the enzyme (fraction II) forming a ternary complex, may be typical for nNOS from most species. Indeed, in preliminary experiments with recombinant human nNOS expressed in the yeast *Pichia pastoris*, a similar heterogeneity was observed (unpublished results). In agreement with a more open substrate binding site in nNOS, we found both association and dissociation rate constants for Arg to be significantly higher than reported for eNOS, whereas substrate affinity was similar.

It is often assumed that K_m(Arg) should be equal to K_d-(Arg). However, even in the case of simple Michaelis−Menten kinetics this presumes rapid-equilibrium substrate binding ($k_d \gg k_{cat}$), which may not always apply. In the present case, the observed dissociation rate constant of 2.5 s^{-1} is in the same range as published values for k_{cat} (2−5 s^{-1}), implying a significant effect of k_{cat} on K_m. Moreover, the rate of association will affect K_m directly, if it is of similar magnitude as k_{cat}. With an association rate constant of 2.5 $\times$ 10^6 $M^{-1}\cdot s^{-1}$ and k_{cat} between 2 and 5 s^{-1} this will occur at a substrate concentration of 1−2 μM, which is in the same range as K_m, indicating that for nNOS the rate of association will become partly rate-limiting at low [Arg]. Consequently, K_m is expected to be somewhat higher than K_d and partly determined by k_{cat} and k_a. A comparison of the values for K_d reported here and elsewhere (0.6−1.0 μM; refs *14*, *17*, and *30*) with published K_m values for nNOS (1−5 μM; for instance, refs *17*, *25*, and *44*−*47*) seems to confirm this.

After this work was completed, a study appeared in which another source for discrepancies between previous observations was proposed, specifically the application of NOS concentrations that were too high to allow proper determination of K_d(Arg) (*48*). As a result, K_d(Arg) may have been overestimated in some cases, and the dependence of K_d(Arg) on imidazole may have been obscured. However, too high concentrations of NOS do not explain the incomplete transition to the high-spin state of the imidazole complex of rat brain nNOS in the presence of Arg, which is evident from the literature (*10*, *17*) and the present study. Therefore, although we concur with the general conclusion of Smith et al. that all NOS isoforms exhibit similar Arg and imidazole binding characteristics (*48*), we maintain that the heterogeneous binding of Arg and imidazole, which is peculiar to nNOS, is the main source of the reported discrepancies. Interestingly, Smith et al. report similar heterogeneity for rat brain nNOS expressed in *E. coli* but not for eNOS, in confirmation of the results reported here (*48*).

We can only speculate about the origin of the heterogeneity observed with rat neuronal nNOS. Although we cannot rigorously rule out protein degradation as a possible cause, the reproducibility with different protein batches, as well as the very similar observations in different laboratories using various expression systems (*10*, *17*, *48*), argues against such an explanation. Moreover, similar observations with the human neuronal isoform expressed in *P. pastoris* demonstrate that the phenomenon is not restricted to a distinct species or expression system. Specifically, the observation of a persistent high-affinity binding fraction (10%) in imidazole titrations in the presence of Arg and BH4, and of an imidazole-induced decrease of the maximally attainable high-spin fraction in Arg titrations (80% with 10 mM imidazole), was replicated with human nNOS (unpublished results). Therefore, it seems that the heterogeneous response represents a bona fide property of the neuronal isoform.

It has been demonstrated repeatedly that certain NOS ligands may adopt multiple binding modes (*28*−*30*, *49*−*51*), bind to more than one site on the enzyme (*34*, *43*, *52*), and form both high-and low-spin complexes (*28*, *53*, *54*). Despite the superficial similarity between those and our observations, such multiplicity of ligand binding cannot explain the heterogeneity of Arg binding, since the distinct enzyme fractions identified by us were not interconvertible. Conversely, NOS heterogeneity may have contributed to the reported multiplicity of ligand binding in some cases.

The observed heterogeneity is reminiscent of the well-documented microheterogeneity found with other members of the cytochrome P450 protein superfamily (cf. refs *55*−*57*), although genetic polymorphism, which underlies most of the heterogeneities reported for cytochrome P450, can be excluded in the case of a recombinant protein. Alternatively, the different species may be due to posttranslational modification. A common source of microheterogeneity is protein glycosylation, but we are unaware of any reports on glycosylation of NOS. To the best of our knowledge, other posttranslational modifications, such as tyrosine nitration, S-nitrosation, or S-glutathiolation, have not been reported either. It has been shown that nNOS can be phosphorylated at various sites, with diverse effects on activity (*58* and references cited therein). However, in the only fully characterized case reported thus far, the phosphorylation site was in the reductase domain, and K_m(Arg) was not affected (*59*). Clearly, elucidation of the basis of the heterogeneous behavior will require further study.

In summary, we found imidazole binding to nNOS to be strongly inhibited by Arg, but not to the extent of mutual exclusivity. The enzyme exhibited heterogeneity with respect

to binding of Arg and imidazole, with a minor part forming a ternary complex. Consequently, imidazole is expected to be a mixed-type inhibitor of nNOS. The equilibrium dissociation constant for Arg was estimated to be approximately 1.0 μM, corresponding to association and dissociation rate constants of 2.5×10^6 $M^{-1}\cdot s^{-1}$ and 2.5 s^{-1}, respectively. The results reported here reconcile apparent discrepancies between previous studies on the interactions between NOS, Arg, and imidazole. Further studies are needed to establish the physiological significance, if any, of the heterogeneity of nNOS revealed here.

REFERENCES

1. Griffith, O. W., and Stuehr, D. J. (1995) *Annu. Rev. Physiol. 57*, 707−736.
2. Mayer, B., and Hemmens, B. (1997) *Trends Biochem. Sci. 22*, 477−481.
3. Gorren, A. C. F., and Mayer, B. (1998) *Biochemistry (Moscow) 63*, 734−743.
4. Stuehr, D. J. (1999) *Biochim. Biophys. Acta 1411*, 217−230.
5. Pfeiffer, S., Mayer, B., and Hemmens, B. (1999) *Angew. Chem., Int. Ed. 38*, 1714−1731.
6. Alderton, W. K., Cooper, C. E., and Knowles, R. G. (2001) *Biochem. J. 357*, 593−615.
7. McMillan, K., Bredt, D. S., Hirsch, D. J., Snyder, S. H., Clark, J. E., and Masters, B. S. S. (1992) *Proc. Natl. Acad. Sci. U.S.A. 89*, 11141−11145.
8. Stuehr, D. J., and Ikeda-Saito, M. (1992) *J. Biol. Chem. 267*, 20547−20550.
9. Rodríguez-Crespo, I., Gerber, N. C., and Ortiz de Montellano, P. R. (1996) *J. Biol. Chem. 271*, 11462−11467.
10. McMillan, K., and Masters, B. S. S. (1993) *Biochemistry 32*, 9875−9880.
11. Gorren, A. C. F., List, B. M., Schrammel, A., Pitters, E., Hemmens, B., Werner, E. R., Schmidt, K., and Mayer, B. (1996) *Biochemistry 35*, 16735−16745.
12. Sennequier, N., and Stuehr, D. J. (1996) *Biochemistry 35*, 5883−5892.
13. Ghosh, D. K., Wu, C., Pitters, E., Moloney, M., Werner, E. R., Mayer, B., and Stuehr, D. J. (1997) *Biochemistry 36*, 10609−10619.
14. Matsuoka, A., Stuehr, D. J., Olson, J. S., Clark, P., and Ikeda-Saito, M. (1994) *J. Biol. Chem. 269*, 20335−20339.
15. Ghosh, D. K., and Stuehr, D. J. (1995) *Biochemistry 34*, 801−807.
16. Chen, P.-F., Tsai, A.-L., Berka, V., and Wu, K. K. (1996) *J. Biol. Chem. 271*, 14631−14635.
17. Roman, L. J., Sheta, E. A., Martasek, P., Gross, S. S., Liu, Q., and Masters, B. S. S. (1995) *Proc. Natl. Acad. Sci. U.S.A. 92*, 8428−8432.
18. Chabin, R. M., McCauley, E., Calaycay, J. R., Kelly, T. M., MacNaul, K. L., Wolfe, G. C., Hutchinson, N. I., Madhusudanaraju, S., Schmidt, J. A., Kozarich, J. W., and Wong, K. K. (1996) *Biochemistry 35*, 9567−9575.
19. Berka, V., Chen, P.-F., and Tsai, A.-L. (1996) *J. Biol. Chem. 271*, 33293−33300.
20. Abu-Soud, H. M., Wang, J., Rousseau, D. L., and Stuehr, D. J. (1999) *Biochemistry 38*, 12446−12451.
21. Mayer, B., Klatt, P., Werner, E. R., and Schmidt, K. (1994) *FEBS Lett. 350*, 199−202.
22. Wolff, D. J., Lubeskie, A., and Umansky, S. (1994) *Arch. Biochem. Biophys. 314*, 360−366.
23. Wolff, D. J., Datto, G. A., Samatovicz, R. A., and Tempsick, R. A. (1993) *J. Biol. Chem. 268*, 9425−9429.
24. Wolff, D. J., and Gribin, B. J. (1994) *Arch. Biochem. Biophys. 311*, 293−299.
25. Harteneck, C., Klatt, P., Schmidt, K., and Mayer, B. (1994) *Biochem. J. 304*, 683−686.
26. Mayer, B., Klatt, P., Harteneck, C., List, B. M., Werner, E. R., and Schmidt, K. (1996) *Methods Neurosci. 31*, 130−139.
27. List, B. M., Klatt, P., Werner, E. R., Schmidt, K., and Mayer, B. (1996) *Biochem. J. 315*, 57−63.
28. Salerno, J. C., Frey, C., McMillan, K., Williams, R. F., Masters, B. S. S., and Griffith, O. W. (1995) *J. Biol. Chem. 270*, 27423−27428.
29. Tsai, A.-L., Berka, V., Chen, P.-F., and Palmer, G. (1996) *J. Biol. Chem. 271*, 32563−32571.
30. Martásek, P., Miller, R. T., Liu, Q., Roman, L. J., Salerno, J. C., Migita, C. T., Raman, C. S., Gross, S. S., Ikeda-Saito, M., and Masters, B. S. S. (1998) *J. Biol. Chem. 273*, 34799−34805.
31. Gorren, A. C. F., Schrammel, A., Schmidt, K., and Mayer, B. (1998) *Biochem. J. 331*, 801−807.
32. Berka, V., and Tsai, A. (2000) *Biochemistry 39*, 9373−9383.
33. Crane, B. R., Arvai, A. S., Ghosh, D. K., Wu, C., Getzoff, E. D., Stuehr, D. J., and Tainer, J. A. (1998) *Science 279*, 2121−2126.
34. Raman, C. S., Li, H., Martásek, P., Král, V., Masters, B. S. S., and Poulos, T. L. (1998) *Cell 95*, 939−950.
35. Salerno, J. C., Martasek, P., Roman, L. J., and Masters, B. S. S. (1996) *Biochemistry 35*, 7626−7630.
36. Crane, B. R., Arvai, A. S., Ghosh, S., Getzoff, E. D., Stuehr, D. J., and Tainer, J. A. (2000) *Biochemistry 39*, 4608−4621.
37. Sennequier, N., Wolan, D., and Stuehr, D. J. (1999) *J. Biol. Chem. 274*, 930−938.
38. Klatt, P., Schmidt, K., Lehner, D., Glatter, O., Bächinger, H. P., and Mayer, B. (1995) *EMBO J. 14*, 3687−3695.
39. Abu-Soud, H. M., Loftus, M., and Stuehr, D. J. (1995) *Biochemistry 34*, 11167−11175.
40. Klatt, P., Pfeiffer, S., List, B. M., Lehner, D., Glatter, O., Bächinger, H. P., Werner, E. R., Schmidt, K., and Mayer, B. (1996) *J. Biol. Chem. 271*, 7336−7342.
41. List, B. M., Klösch, B., Völker, C., Gorren, A. C. F., Sessa, W. C., Werner, E. R., Kukovetz, W. R., Schmidt, K., and Mayer, B. (1997) *Biochem. J. 323*, 159−165.
42. Klatt, P., Schmid, M., Leopold, E., Schmidt, K., Werner, E. R., and Mayer, B. (1994) *J. Biol. Chem. 269*, 13861−13866.
43. Crane, B. R., Arvai, A. S., Gachhui, R., Wu, C., Ghosh, D. K., Getzoff, E. D., Stuehr, D. J., and Tainer, J. A. (1997) *Science 278*, 425−431.
44. Mayer, B., Klatt, P., Werner, E. R., and Schmidt, K. (1994) *Neuropharmacology 33*, 1253−1259.
45. Gerber, N. C., and Ortiz de Montellano, P. R. (1995) *J. Biol. Chem. 270*, 17791−17796.
46. Riveros-Moreno, V., Heffernan, B., Torres, B., Chubb, A., Charles, I., and Moncada, S. (1995) *Eur. J. Biochem. 230*, 52−57.
47. Reif, D. W., and McCreedy, S. A. (1995) *Arch. Biochem. Biophys. 320*, 170−176.
48. Smith, S. M. E., Sham, C., Roman, L., Martasek, P., and Salerno, J. C. (2001) *Nitric Oxide 5*, 442−452.
49. Salerno, J. C., McMillan, K., and Masters, B. S. S. (1996) *Biochemistry 35*, 11839−11845.
50. Wang, J., Stuehr, D. J., and Rousseau, D. L. (1997) *Biochemistry 36*, 4595−4606.
51. Raman, C. S., Li, H., Martásek, P., Babu, B. R., Griffith, O. W., Masters, B. S. S., and Poulos, T. L. (2001) *J. Biol. Chem. 276*, 26486−26491.
52. Raman, C. S., Li, H., Martásek, P., Southan, G., Masters, B. S. S., and Poulos, T. L. (2001) *Biochemistry 40*, 13448−13455.
53. Chen, P.-F., Berka, V., Tsai, A.-L., and Wu, K. K. (1998) *J. Biol. Chem. 273*, 34164−34170.
54. Presta, A., Siddhanta, U., Wu, C., Sennequier, N., Huang, L., Abu-Soud, H. M., Erzurum, S., and Stuehr, D. J. (1998) *Biochemistry 37*, 298−310.
55. Johnson, E. F., and Schwab, G. E. (1984) *Xenobiotica 14*, 3−18.
56. Garda, H. A., Kruger, V., Sidhu, J., and Stier, A. (1994) *Mol. Cell. Biochem. 141*, 1−7.
57. Jansson, I., Mole, J. E., and Schenkman, J. B. (1995) *Arch. Biochem. Biophys. 316*, 275−284.
58. Nathan, C., and Xie, Q. (1994) *J. Biol. Chem. 269*, 13725−13728.
59. Hayashi, Y., Nishio, M., Naito, Y., Yokokura, H., Nimura, Y., Hidaka, H., and Watanabe, Y. (1999) *J. Biol. Chem. 274*, 20597−20602.

BI025675O